IEEE Robotics and Automation Letters (RA-L) paper, presented at ICRA 2026, Vienna, Austria. Cite as RA-L paper.

Energy-based Kinematic Analysis on Magnetic Soft Continuum Robot with Asymmetric Magnetization

Junyeong Lee†, Joowon Park†, and Sukho Park*, *Member, IEEE*

***Abstract*—Magnetically actuated soft continuum robots (MSCRs), which offer remote and wireless control via external magnetic fields along with high flexibility, have recently emerged as a promising technology for minimally invasive surgery (MIS). However, the magnetic actuation forces of MSCRs are generally limited, resulting in inherent workspace constraints. To overcome these limitations, various design strategies have been explored, including the development of an asymmetric magnetized soft continuum robot (AMSCR). Although AMSCRs have demonstrated a significantly larger workspace than conventional MSCRs, a quantitative relationship between the magnetization patterns of embedded magnetic particles and the resulting workspace has not yet been fully clarified. In this study, an energy-based kinematic analysis of AMSCR was conducted to address this issue. Specifically, the equilibrium posture of the AMSCR was determined by minimizing the total potential energy, considering different combinations of external magnetic field directions and internal magnetization patterns. Based on the resulting potential energy graph, the workspace of the AMSCR was quantitatively analyzed, and an optimal linear asymmetric magnetization pattern was identified. Furthermore, the proposed energy-based kinematic model was validated through finite element analysis (FEA) conducted using COMSOL Multiphysics, as well as through experiments performed on a fabricated AMSCR prototype. As a result, an optimal magnetization design method for linearly asymmetric AMSCRs was proposed and experimentally confirmed. The proposed approach is expected to be further applicable to the kinematic performance evaluation and design optimization of AMSCRs with various other magnetization patterns.**

***Index Terms*— Soft continuum robot, Steerable needle, Magnetic actuation, Workspace expansion**

I. Introduction

Minimally invasive surgery (MIS) demands surgical instruments that provide precise control and flexible movement through complex anatomical pathways inside the human body. Continuum robots, which feature continuous mechanical structures without discrete joints, have been proposed as promising solutions for MIS due to their snake-like flexibility and ability to operate within confined spaces [1], [2], [3], [4]. Among these, mechanically actuated continuum robots, which rely on tendon-driven mechanisms, pneumatic systems, or concentric tubes, can achieve highly precise motions. However, these robots often involve bulky and complex designs, which can hinder their effectiveness in the constrained environments typical of surgical applications [5], [6], [7], [8]

To overcome these limitations, magnetically actuated soft continuum robots (MSCRs) have emerged as a promising alternative. MSCRs are typically composed of flexible elastomers embedded with magnetic materials, most often utilizing biocompatible silicone-based polymers such as Ecoflex or PDMS, and can be actuated remotely using external magnetic fields. Compared to conventional mechanically actuated continuum robots, MSCRs possess simpler structures and smaller volumes, making them particularly suitable for operation in confined and complex environments, such as inside blood vessels [9], [10], [11].

Early MSCRs employed simple magnetization strategies, such as attaching one or two permanent magnets at the distal end or uniformly embedding magnetic particles throughout the soft body [12], [13], [14], [15], [16]. For instance, Kim et al. developed a ferromagnetic soft continuum robot with uniformly dispersed magnetic particles and experimentally demonstrated its ability to navigate narrow pathways [17]. However, MSCRs utilizing discrete magnets or uniformly distributed particles often fail to exploit workspace or bending performance, as such simple magnetization patterns do not maximize the generated magnetic torque or resultant curvature. Consequently, for enhanced MSCR performance, factors such as material properties, magnetization distribution, and geometric configuration must be carefully considered, and effective modeling and optimization tools are essential.

Various approaches have been explored to address these limitations. Wang et al. developed a nonuniform magnetization pattern optimized via a genetic algorithm, demonstrating through simulations that such MSCRs could achieve significantly larger workspaces compared to conventional designs [18]. Nevertheless, the fabrication and experimental validation of these MSCRs remain significant challenges. Additionally, shape-programmable MSCRs have been introduced by designing patterned magnetization domains. Pittiglio et al. demonstrated that MSCRs with spatially varying magnetization designed based on CT-imaged anatomical paths could be deformed into pre-programmed

Received 23 July 2025; accepted 15 November 2025. Date of publication 11 December 2025; date of current version 23 December 2025. This article was recommended for publication by Associate Editor J. Qu and Editor B. Mazzolai upon evaluation of the reviewers' comments. This work was supported in part by the National Research Foundation of Korea (NRF), funded by the Ministry of Science and ICT under Grant NRF-2021R1A2C3007817 and the Ministry of Education under Grant RS-2025-25420118, and in part by the Industrial Strategic Technology Development Program, funded by the Ministry of Trade, Industry and Energy (MOTIE, Korea) under Grant 20017903. (Junyeong Lee and Joowon Park contributed equally to this work.)

Junyeong Lee and Sukho Park are with MBR Laboratory, DGIST, Daegu 42988, South Korea (e-mail: junyeong7112@dgist.ac.kr; shpark12@dgist.ac.kr). Joowon Park is with the University of Ulsan, Ulsan 44610, South Korea (e-mail: jwpark12@ulsan.ac.kr).

This article has supplementary downloadable material available at https://doi.org/10.1109/LRA.2025.3643268, provided by the authors.

Digital Object Identifier 10.1109/LRA.2025.3643268

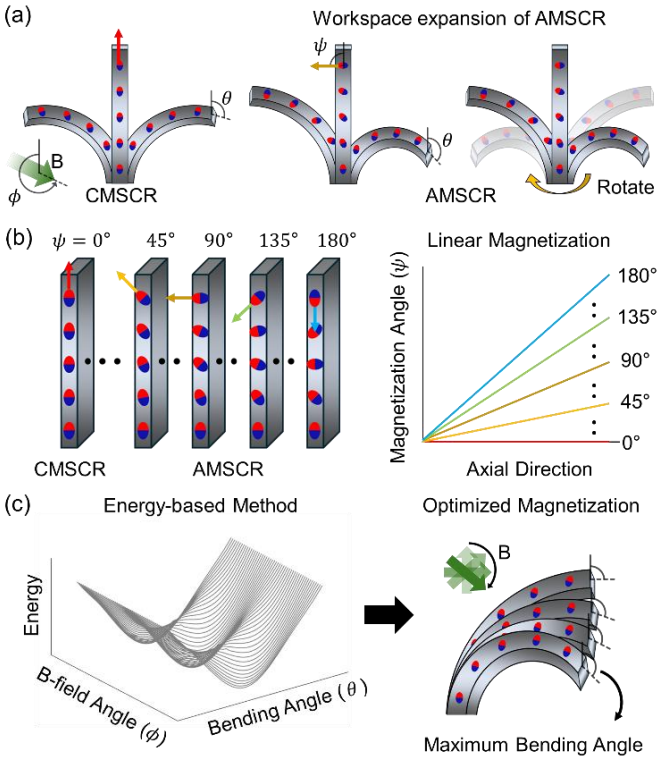

Fig. 1. (a) Concept of CMSCR and AMSCR, (b) Linear magnetization patterns of MSCR, and (c) Magnetization pattern optimization via energy-based analysis.

complex shapes [19]. However, practical limitations are posed by the limited adaptability to diverse surgical scenarios and the complexity of the magnetization process.

Lastly, the asymmetric magnetized soft continuum robot (AMSCR) utilizing an asymmetric magnetization pattern was investigated [20]. As illustrated in Fig. 1(a), the AMSCR exhibits directionally biased bending compared to the conventional magnetized soft continuum robot (CMSCR). Experimental results have demonstrated that this asymmetric design enhances bending performance and expands the available workspace through the utilization of the rotatable nature of MSCRs. However, prior studies assumed a linear magnetization pattern increasing up to 90° without performing detailed analyses or optimizing the resulting workspace. These studies highlight the critical influence of magnetization patterns on workspace and dexterity, yet quantitative analysis and optimization of their relationship have not been sufficiently addressed.

To overcome these limitations, we propose an energy-based kinematic analysis of the AMSCR. As discussed above, previous studies either did not analyze the optimization of magnetization patterns or concentrated on patterns that were difficult to fabricate, thereby restricting experimental validation. Accordingly, the objective of this study is to systematically analyze and optimize the magnetization pattern of the AMSCRs using a readily fabricable linear magnetization configuration. Specifically, as shown in Fig. 1(b), a linear asymmetric magnetization pattern, in which the magnetization angle (ψ) gradually increases along the robot length, is employed. Using the energy-based analysis method illustrated in Fig. 1(c), the bending behavior of the AMSCR is formulated as an energy minimization problem, enabling the prediction of the equilibrium configuration that defines the final deformed state. The objective is to derive an optimal magnetization pattern that maximizes the bending performance of the AMSCR. Specifically, the contributions can be summarized as follows: (1) We propose an energy-based kinematic analysis framework that quantitatively predicts the bending behavior and workspace of the AMSCR. (2) The effectiveness of the proposed method is validated through finite element analysis (FEA) and experiments, demonstrating the feasibility of the AMSCR with the optimized magnetization pattern.

This paper is organized as follows: Section 2 details the energy-based modeling approach for MSCRs, the finite element analysis (FEA) procedures, and the experimental setup. Section 3 presents the analysis results and validates the proposed method by comparing it with experimental observations. Section 4 discusses the equivalence and limitations of the proposed magnetization pattern and suggests directions for future research. Finally, Section 5 summarizes the conclusions.

II. Methodology

A. Energy-Based Modeling

In this study, the bending behavior of the magnetically soft continuum robot (MSCR) was analyzed using a hard-magnetic soft rod model embedded with magnetic particles. As shown in Fig. 2(a), the MSCR was modeled by dividing it into n discrete segments. The bending of the MSCR is governed by the magnetic torque generated by the interaction between the external magnetic field (with magnitude B and direction ϕ) and the internal magnetization vector (with magnitude M and direction ψ). The equilibrium configuration of the MSCR is determined as the configuration that minimizes the sum of elastic energy ($E_{elastic}$) and magnetic energy ($E_{magnetic}$). Accordingly, the total potential energy (E_{total}) of the AMSCR is expressed as follows:

$$E_{elastic} = \int_0^{\theta_n} \boldsymbol{\tau}(\theta) d\theta \approx \frac{1}{2}\frac{EA}{\delta}\sum_{i=1}^{n}(\theta_i - \theta_{i-1})^2 \quad (1)$$

$$E_{magnetic} = -\sum_{i=1}^{n} \boldsymbol{M_i} \cdot \boldsymbol{B} = -\sum_{i=1}^{n} |\boldsymbol{M_i}||\boldsymbol{B}| \cos(\phi - \theta_i - \psi_i) \quad (2)$$

$$E_{total} = E_{elastic} + E_{magnetic} \quad (3)$$

Here, τ denotes the bending moment acting on the rod, E represents the Young's modulus, and A is the cross-sectional area. The Young's modulus of the PDMS (20% vol. NdFeB mixture) used in this study was estimated to be approximately 3 MPa based on the referenced literature, while the cross-sectional area was determined from the measured dimensions of the fabricated specimen (3 mm × 1 mm) [21], [22]. δ denotes the length of each segment and is calculated as $\delta = L/n$, where L represents the total length of the MSCR. Elastic energy refers to the energy stored due to angular

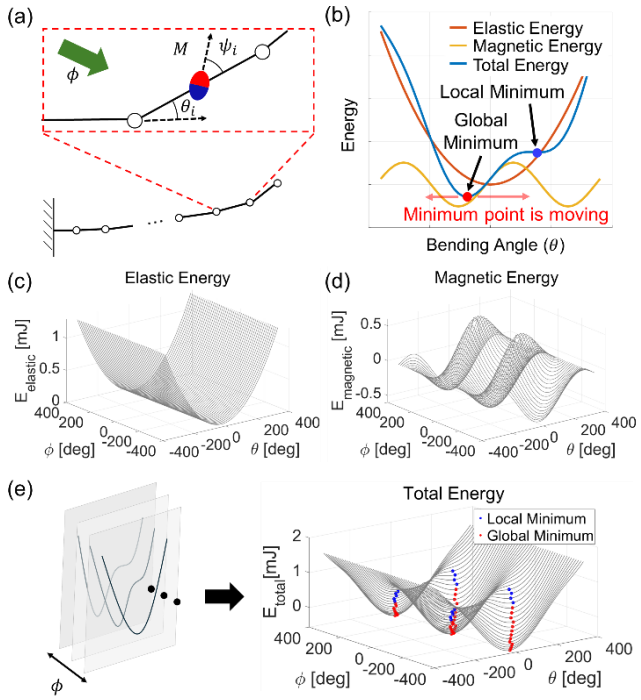

Fig. 2. (a) Model of a MSCR single segment, (b) energy of the MSCR at a specific ϕ, (c) elastic energy of the MSCR, (d) magnetic energy of the MSCR, and (e) total energy of the MSCR with respect to changes in ϕ.

deformation between neighboring segments, whereas magnetic energy arises from the interaction between the internal magnetization direction and the applied external magnetic field. Because the bending angles $(\theta_1, \theta_2, \dots, \theta_n)$ and the magnetization angles $(\psi_1, \psi_2, \dots, \psi_n)$ are interdependent, numerical iterative optimization is required to obtain the optimal bending shape for a given magnetic field direction (ϕ). In this study, MATLAB's fmincon function was employed to determine the optimal equilibrium posture that minimizes the total energy. For a given external magnetic field direction (ϕ) and an assumed final bending angle (θ_n), the optimal equilibrium configuration $(\theta_1, \theta_2, \dots, \theta_{n-1})$ was computed by minimizing the total energy. In the optimization performed using MATLAB's fmincon function, the initial configuration was set to a straight posture, with all $\theta_1, \theta_2, \dots, \theta_{n-1}, \theta_n$ initialized to 0. To balance modeling accuracy and computational efficiency, the number of segments was set to $n = 10$. Using a standard desktop computer equipped with an Intel® Core™ i7-9700K CPU @ 3.60 GHz, the computation of the optimal equilibrium posture for a single magnetization pattern took approximately one hour.

Based on the optimized energy analysis, Fig. 2(b) presents the plots of elastic energy, magnetic energy, and total energy for a specific magnetic field angle (ϕ). In the total energy plot, two local minima were observed, indicating that the MSCR can assume stable bending postures at these equilibrium points. As the magnetic field angle (ϕ) varies, the magnetic energy curve shifts, which in turn alters the location of the local minimum and the corresponding bending posture. Figs. 2(c) and 2(d) visualize the variation of elastic energy and magnetic energy, respectively, in three-dimensional space as the magnetic field angle (ϕ) changes from -360° to 360°. The summation of these energy components yields the three-dimensional total energy surface shown in Fig. 2(e). This surface corresponds to the full angular sweep of the energy curves in Fig. 2(b), and the local minima representing stable bending configurations are visualized in 3D as a function of the magnetic field angle. This energy landscape can be effectively utilized to predict the behavior of the MSCR as the external magnetic field direction varies. Through this analysis, the bending configuration of the MSCR can be precomputed for different external magnetic field directions, facilitating effective path planning and motion control.

B. Finite Element Analysis (FEA) Simulation

To conduct a more precise analysis of the bending performance and magnetic actuation characteristics of the MSCR, finite element analysis (FEA) was performed using COMSOL Multiphysics (COMSOL Inc., Stockholm, Sweden). To predict the bending behavior of the MSCR under an externally applied magnetic field, the AC/DC module was utilized to analyze the electromagnetic forces generated within the embedded NdFeB particles, while the Solid Mechanics module was employed to simulate the resulting bending deformation. Within the AC/DC Module, the Maxwell stress tensor method was applied to compute the magnetic forces induced in the MSCR by the external magnetic field. These forces were determined based on the following equations:

$$B = \mu_0(H + M) \tag{4}$$

$$F_{Mag} = \frac{1}{\mu_0} M \oint_S ((B \cdot \hat{n})B - \frac{1}{2}B^2\hat{n})dS \tag{5}$$

where B is the magnetic flux density of the applied external magnetic field, and μ_0, H, and M denote the magnetic permeability of free space, the magnetic field intensity, and the magnetization of the MSCR, respectively. From these equations, the magnetic force acting on the MSCR due to the external magnetic field can be expressed as a function of its bending deformation. In the Solid Mechanics module, the computed magnetic force F_{Mag} is applied to each element of the modeled MSCR, and the displacement of each element is calculated according to the following equation:

$$\frac{d^2(ms)}{dt^2} = F_{Mag} \tag{6}$$

where m denotes the mass of the MSCR, and s represents the displacement. By substituting the magnetic force F_{Mag} obtained via the Maxwell stress tensor into (6), the displacement s of each MSCR element can be computed. Ultimately, through the aforementioned FEA procedure, the bending posture of the MSCR under various magnetization patterns and external magnetic field directions can be accurately predicted.

C. Fabrication of AMSCR

To experimentally validate the performance of the AMSCR, a prototype was fabricated and evaluated. As shown in Fig. 3(a), the fabrication process proceeded through the following steps: (i) NdFeB magnetic particles (MQFP-B-20076-089, Magnequench) were uniformly mixed with PDMS (Sylgard 184 A, Dow Corning, USA) at a 20% volume fraction using a centrifugal mixer (Thinky Mixer ARV-310, MDRROS Co., in

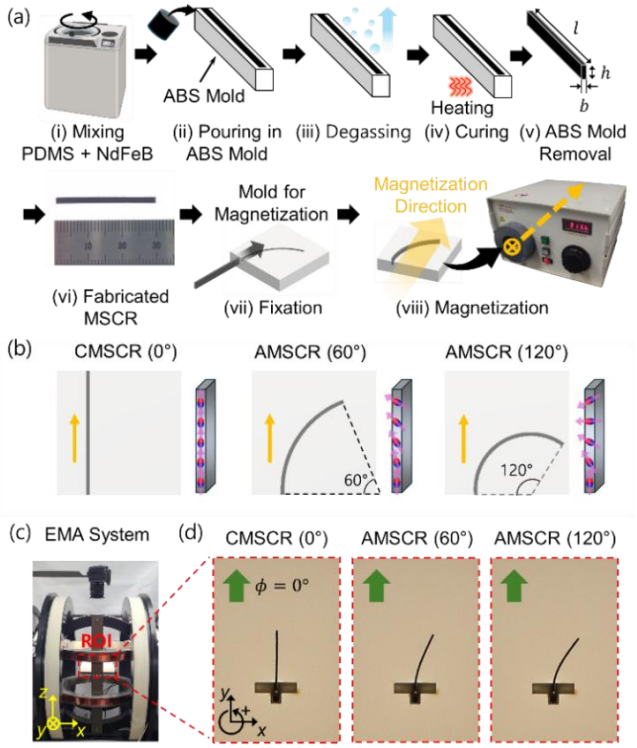

Fig. 3. (a) Fabrication process of the AMSCR, (b) examples of magnetization pattern according to fixation mold, (c) experimental setup, and (d) ROI of the EMA system (20 cm cubic) and posture according to magnetization pattern (ϕ = 0°).

USA). (ii) The resulting mixture was poured into an ABS mold, fabricated via 3D printing, which featured a groove with dimensions of 3 mm in height, 1 mm in width, and 30 mm length. In actual experiments, 5 mm of the MSCR was inserted into the jig, resulting in an effective bending length of 25 mm. (iii) After filling, the mixture was degassed under vacuum. (iv) It was then cured at 80°C for 2 hours. (v) Once cured, the ABS mold was removed, and (vi) the fabricated MSCR was extracted. (vii) To impose the desired magnetization pattern, the MSCR was inserted into a fixation mold shaped as an arc with varying end angles and a fixed length of 30 mm, also produced by 3D printing. (viii) Finally, magnetization was performed using an impulse magnetizer (IM-10-30, ACS Scientific, USA), resulting in an AMSCR with the intended magnetization pattern. Through this procedure, a CMSCR sample with a uniform end magnetization angle of 0°, as well as AMSCR samples exhibiting linearly varying magnetization patterns from 30° to 180° in 30° increments, were fabricated. Additionally, an AMSCR sample with an energy-based optimized linear magnetization pattern was also produced. Fig. 3(b) shows the fixation molds used to generate the desired magnetization patterns, along with the resulting magnetization patterns for the CMSCR (0°) and two AMSCR cases (60° and 120°).

D. Experimental Setup

To validate the magnetic response of the fabricated CMSCR and AMSCR, an experimental setup was constructed as shown in Fig. 3(c). The experimental system utilized an electromagnetic actuation (EMA) platform providing a region of interest (ROI) with a diameter of 20 cm. Within the ROI, a uniform magnetic field with controllable magnitude and direction was generated using three orthogonal pairs of Helmholtz coils. The EMA system was capable of supplying a maximum current of 20 A to each coil, enabling magnetic fields up to 50,000 A/m within the ROI. As shown in Fig. 3(c), a custom experimental jig fabricated via 3D printing was placed inside the ROI, and the CMSCR and AMSCR samples were positioned at the center with one end fixed to ensure consistent boundary conditions. Fig. 3(d) shows the initial positions of the CMSCR and AMSCR samples, which correspond to those described in Fig. 3(b), under a uniform magnetic field of 30,000 A/m oriented at 0°. From these results, it was confirmed that the AMSCR samples exhibited asymmetric magnetization, as designed during the fabrication process. All subsequent experiments and simulations were performed under a magnetic field strength of 30,000 A/m. As illustrated in Fig. 3(c), the +y axis was defined as the 0° reference direction of the magnetic field, and counterclockwise rotation from this axis was considered positive.

III. Results

Fig. 4 presents a comparative analysis of the energy-based method, finite element analysis (FEA), and experimental results for CMSCR and AMSCR, which aims to quantitatively evaluate how the asymmetry in magnetization patterns influences the bending behavior of the continuum soft robot. First, Fig. 4(a) shows the energy map of the CMSCR derived from the energy-based method, shown from a top-down view, illustrating the variation in total energy minimum with respect to the direction of the external magnetic field (ϕ). When the magnetic field direction is 0°, the corresponding equilibrium state is denoted as point 3. As the field rotates in the positive direction, the CMSCR's tip angle begins to bend in the same direction, following a trajectory through local minima from 3 → 4 → 5 on the energy graph. With continued rotation of the magnetic field, the angle between the CMSCR's internal magnetization vector and the external field increases, leading to a rise in magnetic potential. Eventually, this causes the system to become unstable, and the CMSCR undergoes a sudden snapping transition to a new stable posture in the opposite (negative) direction. In the energy map, this is observed as the disappearance of the local minimum at point 5 and an abrupt jump to point 2′, indicating the global energy minimum at that magnetic field direction (ϕ). Due to the symmetric magnetization of the CMSCR, similar behavior also occurs in the negative field direction. That is, as the magnetic field rotates negatively from 0°, the CMSCR sequentially transitions through postures from 3 → 2 → 1 → 4′. Moreover, when starting from point 2′, further rotation in the negative direction leads to a snapping transition through point 1′ back to point 4. Likewise, when starting from point 4′ and rotating the magnetic field in the positive direction, the system snaps through point 5′ and returns to point 2. Snapping behavior occurs not only in the CMSCR but also similarly in the AMSCR. Therefore, the range of θ covering postures 1 to 5 (θ_{max-}=−123°~θ_{max+}=123°) before the snapping points can be defined as the workspace of the CMSCR.

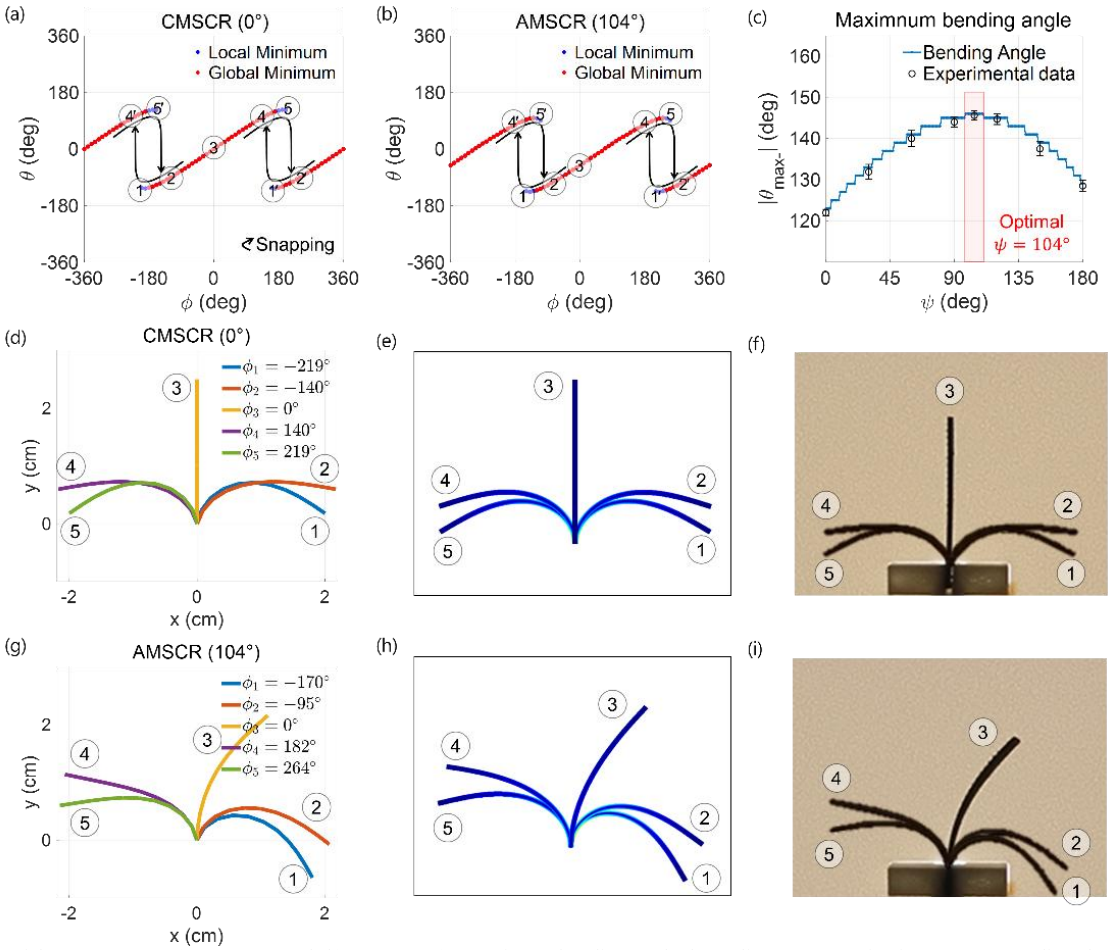

Fig. 4. Top view of the energy map: (a) CMSCR and (b) AMSCR. (c) Maximum bending angle depending on magnetization pattern. Bending shapes of CMSCR according to analysis methods: (d) Energy-based analysis, (e) FEA, and (f) Experiments. Bending shapes of AMSCR according to analysis methods: (g) Energy-based analysis, (h) FEA, and (i) Experiments.

Fig. 4(b) presents the energy map of the AMSCR obtained using the energy-based method, shown from a top view. It illustrates the variation of the total energy local minima with respect to the external magnetic field direction (ϕ) for an AMSCR with a linear magnetization pattern and a tip magnetization angle (ψ) of 104° (as explained in the following section). Similar to the CMSCR, the AMSCR also exhibits snapping behavior in response to changes in the external magnetic field. However, due to the asymmetrical magnetization, the energy map appears biased toward the lower right direction. This indicates that the tip angle of posture 3 at a field direction of 0° is negative, the absolute value of the tip bending angle (θ_{max-})at posture 1 increases, and the absolute value of the tip bending angle (θ_{max+}) at posture 5 decreases. Therefore, in the energy map, the workspace of the AMSCR can be considered as the range of θ up to the snapping points, corresponding to postures 1–5 (θ_{max-}=−148°~θ_{max+}=100°). Nevertheless, the achievable workspace of AMSCR through axial rotation has been considered to span $-|\theta_{max-}|$ to $|\theta_{max-}|$ (-148°~148°), as indicated in [20]. Accordingly, to maximize the workspace of the AMSCR, $|\theta_{max-}|$ should be maximized.

Fig. 4(c) shows the analysis of the maximum bending angle ($|\theta_{max-}|$) of the AMSCR with a linear magnetization pattern as a function of the tip magnetization angle (ψ), obtained using the energy-based method. To validate the energy-based method, experiments were conducted 10 times each on AMSCRs with linear magnetization patterns at 30° intervals (0°, 30°, 60°, 90°, 120°, 150°, and 180°). The analysis using the energy-based method revealed that for AMSCRs with a linear magnetization pattern, the maximum bending angle $|\theta_{max-}|$ was highest within the tip magnetization angle (ψ) range of approximately 98° to 110°, and the intermediate value of 104° was selected as the optimal magnetization angle. Additionally, experiments were performed three times on the AMSCR with a linear magnetization pattern and the optimal tip magnetization angle (ψ = 104°). As previously described, Fig. 4(b) shows the energy map of the AMSCR with a linear magnetization pattern and a tip magnetization angle of 104°.

Fig. 4(d)–(f) show the bending shapes of the CMSCR obtained through the energy-based analytical method, FEA simulation, and experiments, respectively. Similarly, Fig. 4(g)–(i) present the bending shapes of the AMSCR under the same conditions and methods. The bending shapes 1–5 in Fig. 4(d)–(f) correspond to points 1–5 in Fig. 4(a), while the bending shapes 1–5 in Fig. 4(g)–(i) correspond to points 1–5 in Fig. 4(b). From the experimental results (Fig. 4(f) and (i)), it can be observed that the CMSCR exhibits a displacement of approximately −120° to +121° as the external magnetic field direction changes, whereas the AMSCR exhibits a

displacement of approximately −146° to +101°. Because the MSCR can rotate axially, the AMSCR achieves an increase in workspace of about 25° on each side compared to the CMSCR. The bending angles for Fig. 4(d)–(f) are summarized in detail in Table 1, while those for Fig. 4(g)–(i) are summarized in Table 2. The average error between the proposed energy-based method and FEA was found to be approximately 3.08% for the CMSCR and 2.85% for the AMSCR, and the average error with respect to experimental results was approximately 1.42% for the CMSCR and 0.46% for the AMSCR. These results demonstrate that the proposed energy-based method can predict the bending behavior of the MSCR with reasonable accuracy and efficiency. Thus, it can serve as a powerful framework for quantitatively estimating the bending tendencies of MSCRs without the need for complex and computationally intensive FEA simulations.

TABLE I
BENDING ANGLES OF CMSCR

Method	θ_1	θ_2	θ_3	θ_4	θ_5
Energy-based Analysis	-123°	-99°	0°	99°	123°
FEA	-121°	-105°	0°	105°	121°
Experiment	-120°	-97°	0°	98°	121°

TABLE II
BENDING ANGLES OF AMSCR

Method	θ_1	θ_2	θ_3	θ_4	θ_5
Energy-based Analysis	-148°	-125°	-48°	78°	100°
FEA	-150°	-125°	-44°	80°	102°
Experiment	-147°	-127°	-44°	78°	100°

IV. DISCUSSION

A. Analytical Equivalence Between Linear Magnetization Patterns of AMSCR

As examined in the preceding sections, the magnetization pattern of the MSCR constitutes one of the key factors determining its bending behavior, significantly influencing the workspace and actuation stability of the MSCR. However, since implementing excessively complex magnetization patterns is impractical during actual AMSCR fabrication, conducting investigations and analyses on a wide variety of magnetization patterns would be inefficient. Therefore, this study analytically investigates the bending configurations of MSCRs by taking a representative linearly increasing magnetization pattern as a baseline and examining its variations through different transformations. Fig. 5 shows the results of bending and workspace analyses of AMSCRs with a linearly increasing magnetization pattern obtained through energy-based analysis, as well as cases where the linear magnetization pattern is reversed or translated in parallel.

First, Fig. 5(a) presents the AMSCR with the proposed linearly increasing magnetization pattern, the corresponding

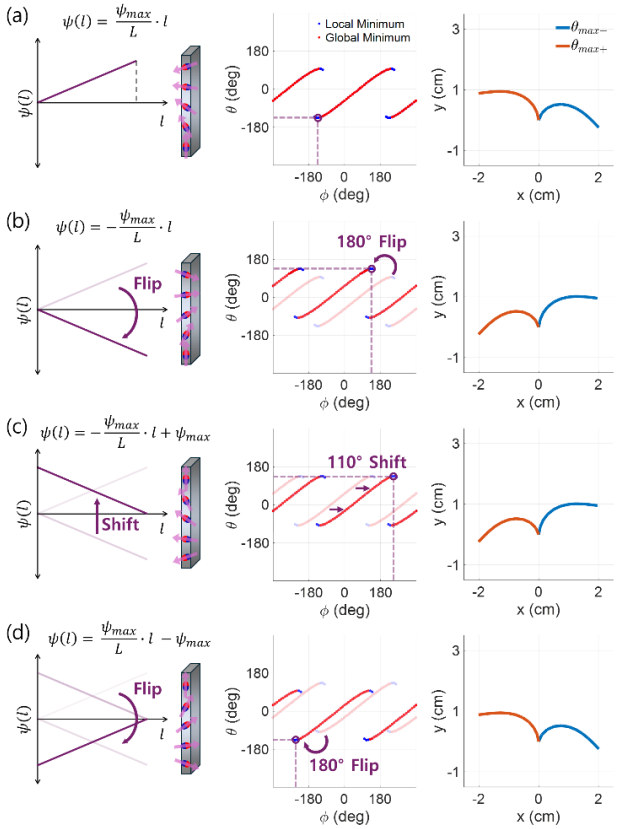

Fig. 5. Analytical equivalence between linear magnetization patterns of AMSCR: (a) Basic pattern, (b) Flipped pattern of (a), (c) Shifted pattern of (b), and (d) Flipped pattern of (c).

energy map, and the maximum bending configurations on both sides (θ_{max-}, θ_{max+}). Second, Fig. 5(b) depicts the case where the magnetization pattern in Fig. 5(a) is horizontally mirrored. Compared to the results in Fig. 5(a), the bending configuration of the AMSCR appears symmetrical, which is confirmed by the energy map being rotated 180° about the origin due to the reversal of the magnetization pattern, and by the mirrored maximum bending shapes of the AMSCR. Third, Fig. 5(c) illustrates the parallel translation of the magnetization pattern from Fig. 5(b), resulting in a monotonic decreasing magnetization pattern. When compared with Fig. 5(b), the bending configurations remain identical, and the energy map is accordingly shifted. Lastly, Fig. 5(d) depicts the magnetization pattern obtained either by reversing the pattern in Fig. 5(c) or by translating the pattern in Fig. 5(a), which yields identical results in both cases. Accordingly, when compared with Fig. 5(c), the bending configuration is symmetrical, and the energy map is rotated 180° about the origin. Conversely, compared to Fig. 5(b), the bending configuration remains the same, and the energy map is translated.

Hence, it is concluded that the deformation of AMSCRs with similar linear monotonic increasing or decreasing magnetization patterns, as shown in Fig. 5, can be analytically predicted through simple transformations of the AMSCR with a linearly increasing magnetization pattern. In summary, by performing reversal and parallel translation operations on a single linearly increasing magnetization pattern, the actuation behaviors of decreasing magnetization patterns can be

TABLE III
FIXATION MOLD EQUATIONS AND BENDING CONFIGURATIONS OF MONOTONICALLY INCREASING MAGNETIZATION PATTERNS

Magnetization Pattern	Fixation Mold Equation	Fixation Mold Design	Maximum Bending Posture
Linear $\psi(l) = \alpha l$, where $\alpha = \frac{\pi}{2L}$ 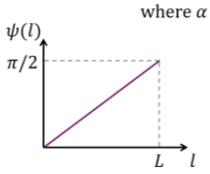	$x(l) = \int_0^l \cos(\alpha s)\, ds = \frac{\sin(\alpha l)}{\alpha}$ $y(l) = \int_0^l \sin(\alpha s)\, ds = \frac{1-\cos(\alpha l)}{\alpha}$	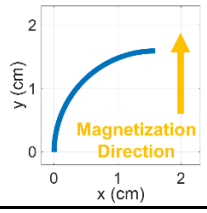	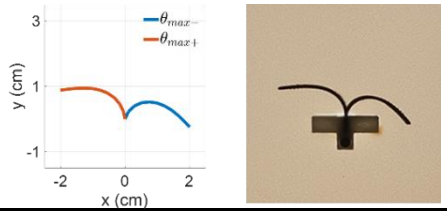
Square $\psi(l) = \alpha l^2$, where $\alpha = \frac{\pi}{2L^2}$ 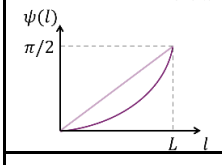	$x(l) = \int_0^l \cos(\alpha s^2)\, ds$ $y(l) = \int_0^l \sin(\alpha s^2)\, ds$	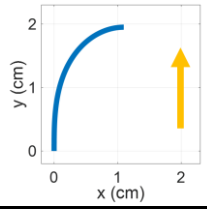	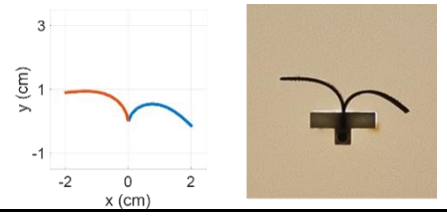
Exponential $\psi(l) = \alpha(e^{l/L} - 1)$, where $\alpha = \frac{\pi}{2(e-1)}$ 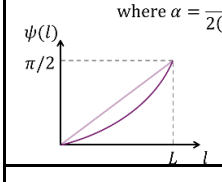	$x(l) = \int_0^l \cos(\alpha(e^{s/L} - 1))\, ds$ $y(l) = \int_0^l \sin(\alpha(e^{s/L} - 1))\, ds$	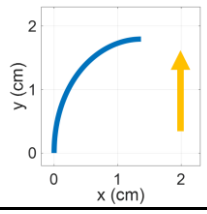	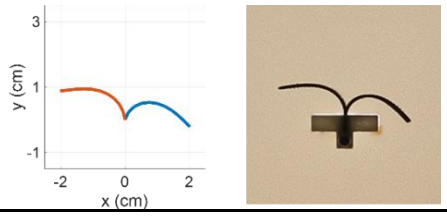
Sinusoidal $\psi(l) = \frac{\pi \sin(\alpha l)}{2}$, where $\alpha = \frac{\pi}{2L}$ 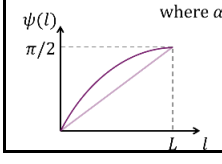	$x(l) = \int_0^l \cos\left(\frac{\pi \sin(\alpha s)}{2}\right) ds$ $y(l) = \int_0^l \sin\left(\frac{\pi \sin(\alpha s)}{2}\right) ds$	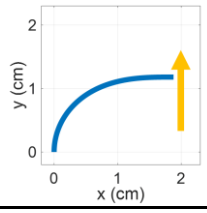	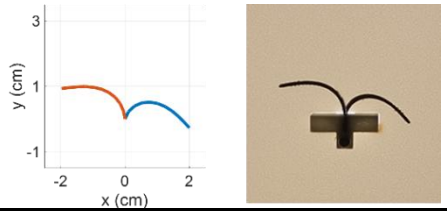

analytically encompassed, establishing equivalence among these magnetization patterns. This enables the overall bending behavior to be inferred without conducting individual analyses for various magnetization patterns, thereby significantly enhancing the efficiency of magnetization design and analysis processes using the proposed energy-based analysis method.

B. Comparison of Monotonically Increasing Magnetization Patterns

In the previous Section 4.1, it was confirmed that the deformation of AMSCRs with various linear magnetization patterns can be predicted through analytical transformations of AMSCRs possessing a monotonically increasing linear magnetization pattern. However, as non-linear magnetization patterns can also be applied to AMSCRs, a comparative analysis of their bending behavior becomes necessary. Particularly, given that more complex patterns increase the challenges of mold design and implementation, it was anticipated that if no significant difference in bending performance is observed among these patterns, simpler magnetization patterns could be preferred.

In this study, not only AMSCRs with linear magnetization patterns but also AMSCRs with three types of monotonically increasing magnetization patterns (square, exponential, and sinusoidal) were analytically compared in terms of bending performance. Table 3 shows the equations for the linear and the three monotonically increasing magnetization patterns for AMSCRs, the magnetization fixation mold equations derived to fabricate these four types of AMSCRs, the corresponding fixation mold designs, and the maximum bending configurations obtained analytically using the energy-based method. Specifically, each magnetization pattern of the AMSCR is expressed by the function $\psi(l)$, which defines the longitudinal distribution of the magnetization angle. By integrating this function, the magnetization mold equation can be derived, indicating how the AMSCR should be arranged in-plane during the magnetization process.

$$x(l) = \int_0^l \cos\big(\psi(s)\big)\, ds \tag{7}$$

$$y(l) = \int_0^l \sin\big(\psi(s)\big)\, ds \tag{8}$$

As shown in Table 3, the magnetization fixation mold equation for the AMSCR with a linear magnetization pattern can be readily derived as the equation of a circle. However, for the other three monotonically increasing magnetization patterns, analytical solutions to the general integral forms are not available, necessitating the design of the actual magnetization fixation molds through numerical integration. Ultimately, Table 3 summarizes the maximum bending angles (θ_{max-}, θ_{max+}) of the four types of AMSCRs, each with a different magnetization pattern. It was confirmed that although these AMSCRs exhibit

different magnetization variation patterns, their maximum bending angles remain nearly identical, differing by approximately up to 5 degrees. Therefore, among the considered AMSCRs with monotonically increasing magnetization patterns, the AMSCR with a linear magnetization pattern can be considered the most favorable choice. This preference arises not only from its analytical simplicity and manufacturing efficiency, but also from the fact that the nonlinear patterns - such as square, exponential, and sinusoidal distributions - demand complex fixation molds and highly precise magnetization processes, while providing only marginal performance gains (approximately within a 5° difference).

V. Conclusion

This study was conducted to systematically approach the design of magnetization patterns from the perspective of energy-based kinematic analysis to maximize the bending performance of AMSCR. In particular, the total potential energy, defined as the sum of elastic and magnetic energies in AMSCR, was quantitatively formulated as an energy minimization problem, through which the maximum bending configuration of the AMSCR could be derived. Using the proposed energy-based analysis method, the optimal magnetization gradient for linear magnetization patterns was obtained, and the workspace difference between the CMSCR and AMSCR with linear magnetization patterns was quantitatively compared under the same conditions. Moreover, when the results of the proposed energy-based analysis method, FEA simulation, and actuation experiments on the fabricated MSCR were compared, a very high degree of agreement was achieved, thereby validating the proposed energy-based analysis approach. As a result, it was confirmed that the AMSCR, with optimized linear magnetization patterns, exhibited an approximately 25° increased maximum bending angle compared to the CMSCR. Additionally, it was shown that monotonic decreasing magnetization patterns can be analytically included simply by reversing or translating a single linear magnetization pattern, thereby enhancing analytical efficiency in predicting the deformation characteristics of MSCR without performing separate analyses for various magnetization patterns. Furthermore, fixation mold equations for AMSCRs with various monotonic increasing magnetization functions, such as square, exponential, and sinusoidal, were derived, and the energy-based analysis of these AMSCRs confirmed that there was no significant difference in bending performance among them. In summary, this study established an energy-based kinematic analysis framework for the design and analysis of MSCRs with asymmetric magnetization patterns and proposed an approach to quantitatively predict and optimize the actuation characteristics and workspace of MSCRs without relying on complex FEA or repetitive experiments. The proposed method has been validated as a practical analysis tool for preoperative optimization of AMSCR magnetization patterns, demonstrating greater computational efficiency than FEA and strong agreement with experimental results. In addition, the proposed approach is expected to serve as a practical design guideline for continuum robot designs requiring precise control in various medical environments. Future work will aim to further reduce computational time to enhance its overall applicability.

References

[1] O. M. Omisore, S. Han, J. Xiong, H. Li, Z. Li, and L. Wang, "A review on flexible robotic systems for minimally invasive surgery," IEEE Trans. Syst., Man, Cybern.: Syst., vol. 52, no. 1, pp. 631–644, 2020.

[2] V. Vitiello, S. L. Lee, T. P. Cundy, and G. Z. Yang, "Emerging robotic platforms for minimally invasive surgery," IEEE Rev. Biomed. Eng., vol. 6, pp. 111–126, 2012.

[3] J. Burgner-Kahrs, D. C. Rucker, and H. Choset, "Continuum robots for medical applications: A survey," IEEE Trans. Robot., vol. 31, no. 6, pp. 1261–1280, 2015.

[4] M. Runciman, A. Darzi, and G. P. Mylonas, "Soft robotics in minimally invasive surgery," Soft Robot., vol. 6, no. 4, pp. 423–443, 2019.

[5] [5] T. da Veiga et al., "Challenges of continuum robots in clinical context: A review," Prog. Biomed. Eng., vol. 2, no. 3, p. 032003, 2020.

[6] Y. J. Kim, S. Cheng, S. Kim, and K. Iagnemma, "A stiffness-adjustable hyperredundant manipulator using a variable neutral-line mechanism for minimally invasive surgery," IEEE Trans. Robot., vol. 30, no. 2, pp. 382–395, 2013.

[7] J. Ding et al., "Design, simulation and evaluation of kinematic alternatives for insertable robotic effectors platforms in single port access surgery," in Proc. IEEE Int. Conf. Robot. Autom. (ICRA), 2010, pp. 1053–1058.

[8] L. B. Kratchman, T. L. Bruns, J. J. Abbott, and R. J. Webster, "Guiding elastic rods with a robot-manipulated magnet for medical applications," IEEE Trans. Robot., vol. 33, no. 1, pp. 227–233, 2016.

[9] I. A. Seleem, H. El-Hussieny, and H. Ishii, "Recent developments of actuation mechanisms for continuum robots: A review," Int. J. Control Autom. Syst., vol. 21, no. 5, pp. 1592–1609, 2023.

[10] J. Hwang, J. Y. Kim, and H. Choi, "A review of magnetic actuation systems and magnetically actuated guidewire-and catheter-based microrobots for vascular interventions," Intell. Serv. Robot., vol. 13, no. 1, pp. 1–14, 2020.

[11] Z. Yang, H. Yang, Y. Cao, Y. Cui, and L. Zhang, "Magnetically actuated continuum medical robots: A review," Adv. Intell. Syst., vol. 5, no. 6, p. 2200416, 2023.

[12] S. Jeong et al., "Feasibility study on magnetically steerable guidewire device for percutaneous coronary intervention," Int. J. Control Autom. Syst., vol. 15, no. 1, pp. 473–479, 2017.

[13] D. Lin, N. Jiao, Z. Wang, and L. Liu, "A magnetic continuum robot with multi-mode control using opposite-magnetized magnets," IEEE Robot. Autom. Lett., vol. 6, no. 2, pp. 2485–2492, 2021.

[14] Y. Kim et al., "Telerobotic neurovascular interventions with magnetic manipulation," Sci. Robot., vol. 7, no. 65, p. eabg9907, 2022.

[15] P. Lloyd, Z. Koszowska, M. Di Lecce, O. Onaizah, J. H. Chandler, and P. Valdastri, "Feasibility of fiber reinforcement within magnetically actuated soft continuum robots," Front. Robot. AI, vol. 8, p. 715662, 2021.

[16] P. Lloyd, O. Onaizah, G. Pittiglio, D. K. Vithanage, J. H. Chandler, and P. Valdastri, "Magnetic soft continuum robots with braided reinforcement," IEEE Robot. Autom. Lett., vol. 7, no. 4, pp. 9770–9777, 2022.

[17] Y. Kim, G. A. Parada, S. Liu, and X. Zhao, "Ferromagnetic soft continuum robots," Sci. Robot., vol. 4, no. 33, p. eaax7329, 2019.

[18] L. Wang et al., "Evolutionary design of magnetic soft continuum robots," Proc. Natl. Acad. Sci. U.S.A., vol. 118, no. 21, p. e2021922118, 2021.

[19] G. Pittiglio et al., "Patient-specific magnetic catheters for atraumatic autonomous endoscopy," Soft Robot., vol. 9, no. 6, pp. 1120–1133, 2022.

[20] J. Park et al., "Magnetically steerable asymmetric magnetized soft continuum robot (AMSCR) for minimally invasive surgery," in Proc. IEEE Int. Conf. Robot. Autom. (ICRA), 2022, pp. 9586–9592

[21] I. D. Johnston, D. K. McCluskey, C. K. L. Tan, and M. C. Tracey, "Mechanical characterization of bulk Sylgard 184 for microfluidics and microengineering," J. Micromech. Microeng., vol. 24, no. 3, p. 035017, 2014.

[22] E. Guth, "Theory of filler reinforcement," J. Appl. Phys., vol. 16, no. 1, pp. 20–25, 1945.